Journal of Nuclear Materials 386–388 (2009) 241–244

Contents lists available at ScienceDirect

Journal of Nuclear Materials

journal homepage: www.elsevier.com/locate/jnucmat

Effects of helium on ductile-brittle transition behavior of reduced-activation ferritic steels after high-concentration helium implantation at high temperature

A. Hasegawa [a,*], M. Ejiri [a], S. Nogami [a], M. Ishiga [a], R. Kasada [b], A. Kimura [b], K. Abe [a], S. Jitsukawa [c]

[a] Department of Quantum Science and Energy Engineering, Tohoku University, 6-6-01-2 Aramaki-aza-Aoba, Aoba-ku, Sendai 980-8579, Japan
[b] Institute of Advanced Energy, Kyoto University, Gokasho, Uji, Kyoto 611-0011, Japan
[c] Japan Atomic Energy Agency, Shirakata-Shirane, Tokai-mura, Ibaraki 319-1195, Japan

A B S T R A C T

The effects of He on the fracture behavior of reduced-activation ferritic/martensitic steels, including oxide dispersion-strengthened (ODS) steels and F82H, was determined by characterizing the microstructural evolution in and fracture behavior of these steels after He implantation up to 1000 appm at around 550 °C. He implantation was carried out by a cyclotron with a beam of 50 MeV α-particles. In the case of F82H, the ductile-to-brittle transition temperature (DBTT) increase induced by He implantation was about 70 °C and the grain boundary fracture surface was only observed in the He-implanted area of all the ruptured specimens in brittle manner. By contrast, no DBTT shift or fracture mode change was observed in He-implanted 9Cr-ODS and 14Cr-ODS steels. Microstructural characterization suggested that the difference in the bubble formation behavior of F82H and ODS steels might be attributed to the grain boundary rupture of He-implanted F82H.

1. Introduction

Reduced-activation ferritic/martensitic (F/M) steels are among the candidate structural materials for the fusion reactor [1]. In the fusion reactor environment, 14 MeV neutron irradiation might produce a large amount of displacement damage and transmutant helium (He) atoms in structural materials. For instance, the displacement damage and He concentration in a F/M steel after 10 MW/m^2 neutron-wall loading will be 100 dpa and 1000 appm, respectively.

The displacement damage might cause a strength increase (irradiation hardening) at temperatures below 400 °C, and this irradiation hardening might reduce the fracture toughness, which would involve an increase in the ductile-brittle transition temperature (DBTT) [1]. It is well known that He can stabilize a point defect cluster and cause additional hardening in the lower temperature region and an increase in swelling in the higher temperature region. He atoms in a material tend to diffuse to form He bubbles at preexisting grain boundaries during high-temperature irradiation and to change the fracture mode from transgranular to intergranular. It is believed that F/M steels have a resistance to He embrittlement owing to their microstructure. A high concentration of He was found not to have a detectable effect on tensile properties up to 600 °C and no grain boundary fracture was observed [2,3].

Oxide dispersion-strengthened (ODS) F/M steels for fuel cladding pipe of fission reactor, which consist of fine grains and ultrafine dispersed oxides, were developed recently [4]. These ODS F/M steels are expected to have a higher strength under high-temperature neutron irradiation than the conventional (non-ODS) F/M steels described above because the grain boundaries and fine dispersed oxides in these materials presumably behave as effective trapping sites and sinks for defects including He [5–7]. The objective of this study is to investigate the effect of He during high-temperature implantation on the impact behavior of ODS F/M steels.

2. Experimental

The materials used in this study were F82H IEA-Heat and two types of ODS steels which were 9Cr- and 14Cr-ODS. These ODS steels were fabricated by a mechanical alloying (MA) process followed by thermo-mechanical treatment. The chemical compositions and the heat treatments of the samples are tabulated in Table 1. The 9Cr-ODS is martensitic-type and the 14Cr-ODS is ferritic-type steels, respectively [8,9]. The miniaturized center V-notch (CVN) specimens for the Charpy impact test were machined to 1.5 × 1.5 × 20 mm, 0.3 mm in notch depth, 0.08 mm in notch root radius and 30° in notch angle.

He ion implantation was performed using 50 MeV α-particles from the AVF cyclotron of CYRIC of Tohoku University. The projected range of 50-MeV He ions in Fe–9Cr steel was calculated to be about 380 μm by TRIM code [10]. A tandem-type energy degrader system was used to obtain the uniform depth distribution of He

* Corresponding author.
E-mail address: akira.hasegawa@qse.tohoku.ac.jp (A. Hasegawa).

0022-3115/$ - see front matter © 2008 Elsevier B.V. All rights reserved.
doi:10.1016/j.jnucmat.2008.12.102

Table 1
The chemical composition of examined steels (unit: wt%).

C	Si	Mn	Cr	W	N	Ti	Al	P	S
F82H									
0.09	0.07	0.1	7.84	1.98	0.007	0.004	0.001	0.003	0.001
Cu	Ni	Mo	V	Nb	B	Co	Ta	Fe	
0.01	0.02	0.03	0.19	0.0002	0.0002	0.003	0.04	Bal.	
IEA Heat No.9753 Roll No.KG820-2									
Normalizing: 1040 °C × 40 min, tempering: 750 °C × 60 min									
C	Si	Mn	Cr	W	N	Ti	Y	Y_2O_3	Fe
9Cr-ODS									
0.14	0.048	0.05	8.67	1.96	0.017	0.23	0.27	0.34	Bal.
Normalizing: 1050 °C × 60 min, AC tempering: 800 °C × 60 min, AC									
C	Si	Mn	Cr	W	N	Ti	Al	Y_2O_3	Fe
14Cr-ODS									
0.04	0.033	0.06	13.64	1.65	0.009	0.28	4.12	0.381	Bal.
Normalizing: 1050 °C × 60 min, AC									

atoms in specimens. The nominal He concentration was about 1000 appm, which was calculated from the beam current. The average displacement damage was about 0.28 dpa. The implantation temperature was 550 ± 10 °C. The Vickers hardness measurement on the irradiated area using 200 gf, instrumented impact test, and fracture surface analysis were carried out after He implantation.

3. Results and discussion

Results of impact tests on F82H, 9Cr-ODS and 14Cr-ODS steels are shown in Figs. 1–3, respectively, and summarized in Fig. 4. Fig. 1 shows the Charpy impact energy vs. temperature curves of F82H before and after He implantation, which reveal that the DBTT increase induced by 1000-appm He implantation was about 70 °C. The Vickers hardness test results indicate a slight hardening ($\Delta Hv = 40$) in the He-implanted area of these specimens. Fig. 5(a) shows a SEM micrograph of the He-implanted specimen that underwent brittle fracture at −60 °C. Grain boundary surface was observed from the bottom of the notch to a depth of about

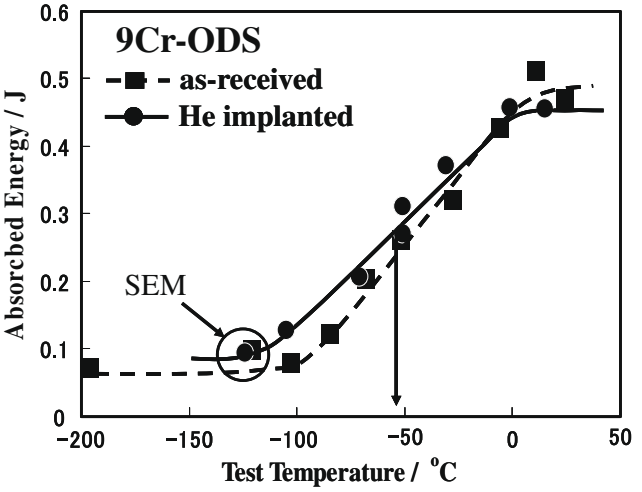

Fig. 2. Charpy impact energy vs. temperature curves of 9Cr-ODS before and after 1000 appm He implantation at 550 °C.

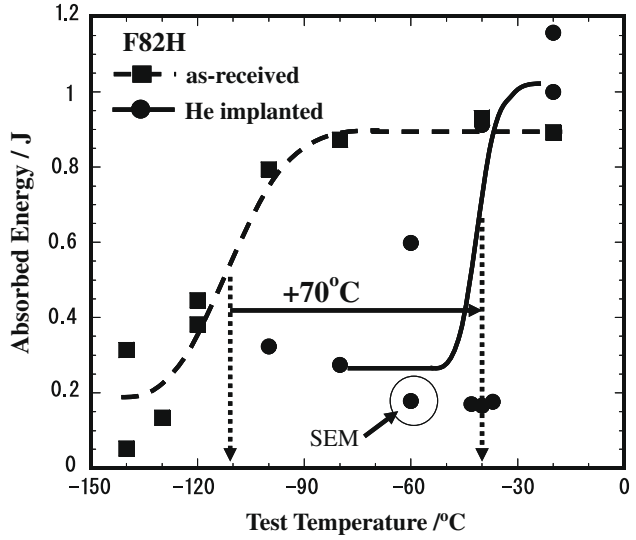

Fig. 1. Charpy impact energy vs. temperature curves of F82H before and after 1000 appm He implantation at 550 °C.

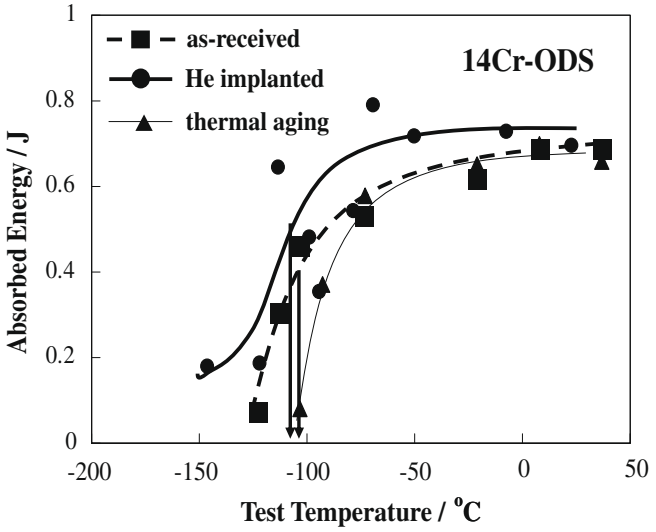

Fig. 3. Charpy impact energy vs. temperature curves of 14Cr-ODS before and after 1000 appm He implantation at 550 °C.

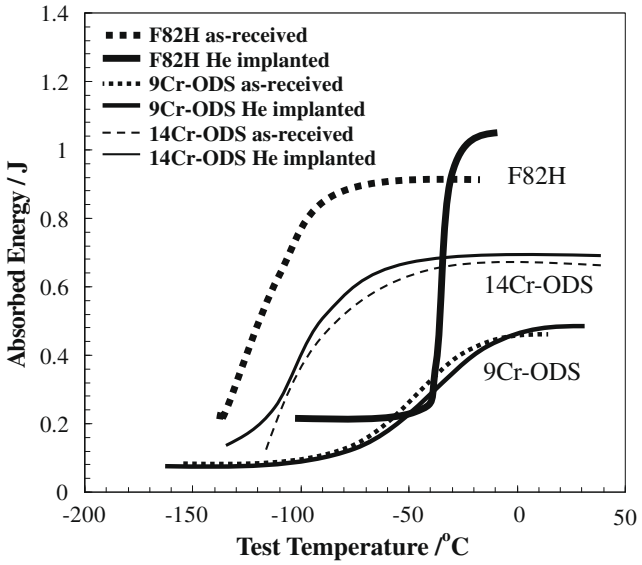

Fig. 4. Summary of Charpy impact energy vs. temperature curves.

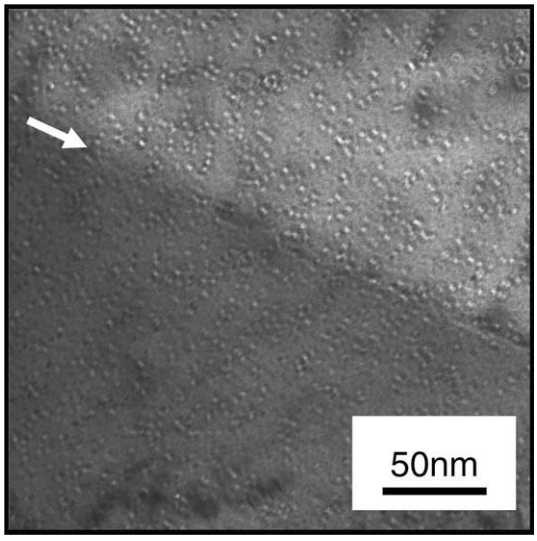

Fig. 6. TEM micrograph of He-implanted 9Cr-ODS. Implanted He: 1000 appm, implanted temperature: 550 °C.

400 μm. This area corresponds to the He-implanted region. No grain boundary ruptured surface was observed in He-implanted specimens that underwent ductile fracture. No studies have dealt with the microstructural characterization of He-implanted specimens to date, except for that by Takahashi et al., who used a TEM to examine the microstructure after 1000-appm He implantation F-82H at 550 °C by DuET and showed He bubble segregation at lath boundary [11]. Thus, grain boundary fracture was presumably initiated by crack formation at the bubble-precipitated boundary.

Fig. 2 shows the Charpy impact data of 9Cr-ODS steel before and after He implantation. It can be seen that He implantation had nearly no effect on the DBTT of this steel. Fig. 5(b) shows the fracture surface of the He-implanted specimen that ruptured in a brittle manner at −120 °C. The fracture mode in the He-implanted and un-implanted regions of the 9Cr-ODS steel was cleavage, and no grain boundary type surface was observed in this work. The hardness of the He-implanted area decreased relative to the un-implanted area ($\Delta Hv = -100$), indicating the possibility of irradiation-induced recovery of the microstructure. Fig. 6 shows TEM micrographs of a He-implanted 9Cr-ODS, which was obtained by 3-MeV He implantation to 1000 appm at 550 °C using the dynamitron-type accelerator at Tohoku University. An arrow in the figure shows grain boundary. Fine bubbles were observed in the matrix. These were found to be distributed uniformly, and no bubble segregation on grain boundaries was observed. This showed that the He trapping capacity induced by oxide particles was still effective after the He implantation. This type of bubble distribution was presumably due to fine precipitates in the matrix and to the fine grain structure of the ODS steels.

The Charpy impact data of 14Cr-ODS are shown in Fig. 3. The DBTT of the as-received and He-implanted 14Cr-ODS steel was −100 °C. No ruptured surface change due to He implantation was observed. The DBTT of 14Cr-ODS steel did not change upon the He implantation but a slight decrease of hardness ($\Delta Hv = -15$) was observed in the He-implanted area. From the view point of microstructure, the 9Cr-ODS has martensitic structure and the 14Cr-ODS has ferritic structure. Both specimens have fine and dense oxide particles [8,9]. Yutani et al. showed He bubble trap-

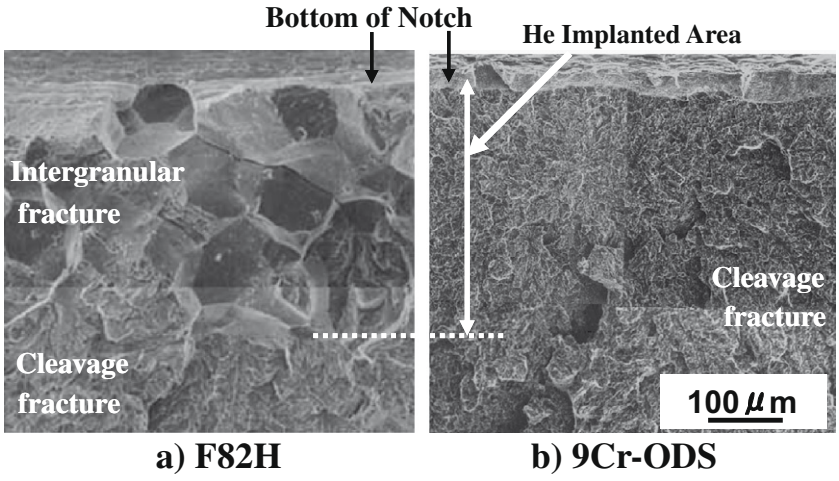

Fig. 5. The typical fracture surfaces for the He-implanted impact test specimen of (a) F82H tested at −60 °C, (b) 9Cr-ODS steel tested at −120 °C.

ping behavior on the fine oxide particles after ion irradiation [12]. These results reveal that fine and dense oxide particle has enough trapping capacity of He to 1000 appm at around 600 °C.

Fig. 4 summarizes the Charpy impact data obtained in this work. DBTT shift was only observed in F82H. In terms of the DBTT shift, the resistance to He embrittlement of F82H is lower than those of 9Cr- and 14Cr-ODS steels. However, the upper shelf of the absorbed energy of ODS steels is lower than that of F82H. Further improvement of mechanical properties is needed to exploit the He embrittlement resistance of ODS steels in applications.

4. Summary

The effect of high-concentration He implanted at 550 °C on the impact test behavior of 9Cr- and 14Cr-ODS steels was compared to that of F82H using high-energy α-particle irradiation by accelerators.

Almost no increase in the DBTT and no intergranular fracture due to He implantation were observed for 9Cr- and 14Cr-ODS steels, while F82H showed both a DBTT increase and intergranular fracture. The finely dispersed oxides and fine grain boundary in these ODS steels are considered to effectively behave as He trapping sites. Suppression of irradiation hardening and grain boundary degradation due to high-concentration He at around 550 °C are anticipated for ODS steels.

Acknowledgements

We are grateful to the staff of CYRIC of Tohoku University in connection with the accelerator operation and irradiation experiments. We are also indebted to the staff of the hot laboratory at the International Research Center for Nuclear Materials Science of IMR, Tohoku University, Oarai, where post-irradiation experiments were carried out.

References

[1] N. Baluc, D.S. Gelles, S. Jitsukawa, A. Kimura, R.L. Klueh, G.R. Odette, B. van der Schaaf, Yu Jinnan, J. Nucl. Mater. 367–370 (2007) 33.
[2] A. Hasegawa, H. Shiraishi, J. Nucl. Mater. 191–194 (1992) 910.
[3] A. Hasegawa, N. Yamamoto, H. Shiraishi, J. Nucl. Mater. 202 (1993) 266.
[4] S. Ukai, M. Fujiwara, J. Nucl. Mater. 307–311 (2002) 749.
[5] R.L. Klueh, P.J. Maziasz, I.S. Kim, L. Heatherly, D.T. Hoelzer, N. Hashimoto, E.A. Kenik, K. Miyahara, J. Nucl. Mater. 307–311 (2002) 773.
[6] R. Schaeublin, T. Leguey, P. Spätig, N. Baluc, M. Victoria, J. Nucl. Mater. 307–311 (2002) 778.
[7] B.N. Goshchitskii, V.V. Sagaradze, V.I. Shalaev, V.L. Arbuzov, Y. Tian, W. Qun, S. Jiguang, J. Nucl. Mater. 307–311 (2002) 783.
[8] S. Ukai, S. Mizuta, M. Fujiwara, T. Okuda, T. Kobayashi, J. Nucl. Sci. Technol. 39 (7) (2002) 778.
[9] H.S. Cho, A. Kimura, S. Ukai, M. Fujiwara, J. Nucl. Mater. 329–333 (2004) 387.
[10] J.P. Biersack, J.F. Ziegler, TRIM85 Program, IBM Corp., Yorktown, NY, 1985.
[11] H. Takahashi, R. Kasada, A. Kimura, Master of thesis, Kyoto University, 2006.
[12] K. Yutani, H. Kishimoto, R. Kasada, A. Kimura, J. Nucl. Mater. 367–370 (2007) 423.